J|A|C|S
COMMUNICATIONS

Published on Web 07/10/2008

Extended Metal-Atom Chains with an Inert Second Row Transition Metal: $[Ru_5(\mu_5\text{-tpda})_4X_2]$ ($tpda^{2-}$ = tripyridyldiamido dianion, X = Cl and NCS)

Caixia Yin,[†,‡,§] Gin-Chen Huang,[†] Ching-Kuo Kuo,[†] Ming-Dung Fu,[||] Hao-Cheng Lu,[†] Jhih-Hong Ke,[†] Kai-Neng Shih,[†] Yi-Lin Huang,[⊥] Gene-Hsiang Lee,[†] Chen-Yu Yeh,[⊥] Chun-hsien Chen,*[,†] and Shie-Ming Peng*[,†,§]

Department of Chemistry, National Taiwan University, Taipei 10617, Taiwan, Key Laboratory of Chemical Biology and Molecular Engineering of Ministry of Education, Institute of Molecular Science, Shanxi University, Taiyuan 030006, China, Institute of Chemistry, Academia Sinica, Taipei 11529, Taiwan, Department of Chemistry, National Tsing Hua University, Hsinchu, Taiwan 30013, and Department of Chemistry, National Chung Hsing University, Taichung, Taiwan 40227, ROC

Received June 30, 2008; E-mail: chhchen@ntu.edu.tw; smpeng@ntu.edu.tw

Nearly two decades after the first reports[1–3] on EMACs (extended metal atom chains), exciting findings[4,5]continue to flourish because of the advances in synthesis to make possible a unique platform for fundamental studies of metal−metal multiple bonds beyond dinuclear complexes. The metal atom chains are collinear and supported by four amine-based ligands such as prototypical and derivatized oligo-α-pyridylamines[4,5] and naphthyridine-modified ones.[6–10] By coordinating the ligands with a variety of metal centers, systematic examination of spectroscopic, electrochemical, magnetic, and electric conductance properties of the homologous series of EMACs are feasible. However, the metal centers in EMACs hitherto are limited to first row transition metals such as Cr,[11–14] Co,[6,15,16] Ni,[1,7–10,16–19] and Cu,[2,3] probably because of their lability over those relatively inert ones with filled 4d or 5d shells.[4,5] Reported herein are a synthetic strategy and characterizations for $[Ru_5(\mu_5\text{-tpda})_4Cl_2]$ (**1**, Figure 1) and $[Ru_5(\mu_5\text{-tpda})_4(NCS)_2]$ (**2**, see Supporting Information for the ORTEP view), the first pentanuclear EMACs of the second-row transition metals.

The rich chemistry[20,21] of ruthenium enables its applications associated with electron and energy transfer.[22,23] Diruthenium complexes bear four formal oxidation states[21,24–26] and exhibit profound spectroscopic features.[27] $[Ru_3(\mu_3\text{-dpa})_4Cl_2]$ (dpa = dipyridylamido anion) is our first attempt to explore ruthenium EMACs. The characterization of the physical properties was, however, hampered by a low yield of 2%.[28] Very recently we improved the yield to 53% that allowed the studies[29] of the Ru−Ru distances, spin states, and the spectroelectrochemistry of $[Ru_3]^{6+/7+/8+}$. The key to the success was the addition of an excess amount of LiCl, prior to metalation, to reflux with the starting materials, H_2dpa and $Ru_2(OAc)_4Cl$. The metalation was then activated by a base, *t*-BuOK, and ferrocenium tetrafluoroborate was employed to confer a stable product, $[Ru_3(\mu_3\text{-dpa})_4Cl_2][BF_4]$ (yield 53%). Subsequent reduction by hydrazine yielded the neutral triruthenium EMAC (63%).[29] However, the preparation of $[Ru_5]^{10+}$ EMACs by the same protocol resulted in a low yield (<1%) of an oxidized pentaruthenium, $[Ru_5(\mu_5\text{-tpda})_4Cl_2]$ $\{[Ru_2(OAc)_4Cl]_2Cl\}$ (**3**, see Supporting Information for the ORTEP view).[30] In this present study we discover that a 10% yield of **1** can be achieved by swapping the sequence of metalation and the introduction of LiCl under reflux conditions where the latter impedes the ruthenium-acetate complexation and facilitates the formation of $[Ru_5]^{10+}$.

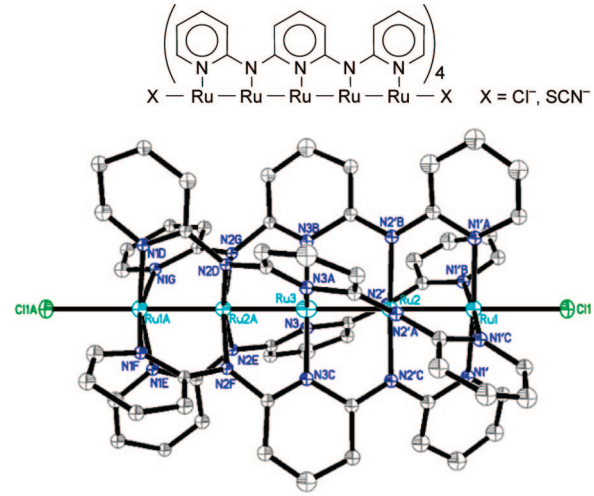

Figure 1. (Top) the metal atom chain is supported by four oligo-α-pyridylamine ligands. (Bottom) ORTEP view of $[Ru_5(\mu_5\text{-tpda})_4Cl_2]$ (**1**). Label A represents symmetric related positions. Thermal ellipsoids are drawn at the 30% probability level. Ru, aqua blue; N, blue; Cl, green; C, gray. The hydrogen atoms are not shown for clarity.

The crystal structure of **1** (Figure 1) shows a linear $[Ru_5]^{10+}$ unit helically coordinated by four $tpda^{2-}$ ligands, the same as the family of pentanuclear EMACs.[4,5,16] *I*4/*m* space group is used for the final refinement with the Ru(3) atom sitting at the crystallographic 2-fold axis which appears slightly elongated. The atomic positions of the compound are averaged owing to the cocrystallization of the right- and left-turn helical forms. Therefore, accurate Ru−N distances are unavailable. Nevertheless, the bond length is in the order of $[Ru(1)-N_{py,outer}] > [Ru(2)-N_{amido}] \approx [Ru(3)-N_{py,inner}]$, ascribed to a smaller negative charge at $N_{py,outer}$ than those at the other nitrogen atoms. The Ru−Cl distance is found to be 2.550(4) Å, shorter than the corresponding 2.596(1) Å of $[Ru_3(dpa)_4Cl_2]$.[29] There are two types of Ru−Ru bond lengths where the outer and inner ones are, respectively, 2.2827(17) and 2.2759(13) Å, slightly longer than the 2.2537(5) Å of $[Ru_3(dpa)_4Cl_2]$.[29]

EPR of **1** was silent, consistent with an even number of electrons for the $[Ru_5]^{10+}$. Figure 2 displays the paramagnetic behavior that the thermal magnetic susceptibility (χ_M) increases at low temperatures. At room temperature, the effective magnetic moment (μ_{eff}) is 2.82 μ_B, corresponding to that of the triplet state composed of two unpaired electrons. Upon cooling, μ_{eff} decreases gradually,

[†] National Taiwan University.
[‡] Shanxi University.
[§] Academia Sinica.
[||] National Tsing Hua University.
[⊥] National Chung Hsing University.

10.1021/ja8016818 CCC: $40.75

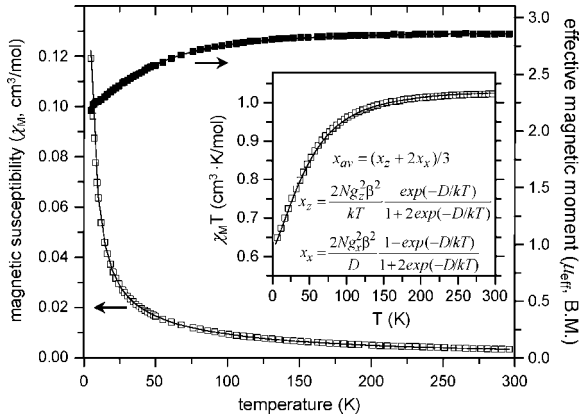

Figure 2. Temperature-dependence of μ_{eff} (■, right axis) and molar magnetic susceptibility χ_M (□, left axis) for compound **1**. (Inset) plot of $\chi_M T$ vs T and its fit according to the Heisenberg model (solid line).

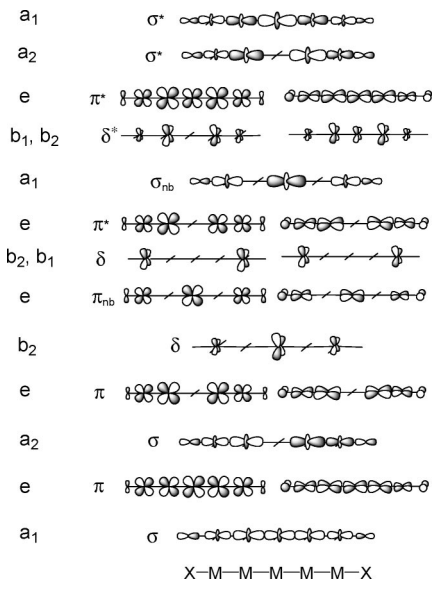

Figure 3. MO diagram of $[Ru_5(\mu_5\text{-tpda})_4(Cl)_2]$. Only orbitals at the $[Cl-Ru_5-Cl]^{8+}$ moiety are highlighted. See Supporting Information for computational details.

indicative of a strong zero field splitting parameter. Theoretical fitting was performed according to the full spin Hamiltonian for an $S = 1$ system with an axial zero-field splitting, $H = g_u\beta S_u H_u + D[S_z^2 - S(S+1)/3]$, where the subscript u denotes the direction of the applied magnetic field.[31] The equations derived from this Hamiltonian are provided in the inset of Figure 2 where the averaged magnetic susceptibility of $x_{av} = (x_z + 2x_x)/3$ is listed. The fitting resulted in 2.16, 1.96, and -112 cm^{-1} for $g_\perp$, $g_{||}$, and the zero-field splitting parameter D, respectively. One possibility for such a strong D is that the experiments were carried out with powder samples due to the difficulty in growing sufficiently large crystals. Because the measurements are significantly affected by the relative orientation of the crystalline plane to the direction of the magnetic field, we are uncertain about whether the isotropic model is suitable although the fitting results appear superb ($R^2 = 0.99952$).

DFT/B3LYP analysis of **1** was carried out with Gaussian 03w package using LANL2DZ on Ru, D95V on C, H, and D95* on N, Cl. The orbitals at the metal centers are drawn in Figure 3. The ground-state of **1** is found to be $^3A_2$ with an electronic configuration of $Q^{22}\pi^{*4}\sigma_{nb}{}^2\delta^{*1}\delta^{*1}$ where Q^{22} represents $\sigma^2\pi^4\sigma^2\pi^4\delta^2\pi_{nb}{}^4\delta^2\delta^2$ and the last two electrons in the $\delta^{*1}\delta^{*1}$ are filled, corresponding to the paramagnetic behavior found in Figure 2. The bond order between the adjacent Ru^{2+} is 1. For comparison with its analogue, $[Ru_3(dpa)_4Cl_2]$, our previous DFT study showed an electronic configuration of $\sigma^2\pi^4\delta^2\pi_{nb}{}^4\delta_{nb}{}^2\delta^{*2}\sigma_{nb}{}^2$, resulting in the characteristics of diamagnetism and an Ru−Ru bond order of 1.5.[29]

The voltammogram of complex **1** exhibited five reversible waves at -0.71, -0.11, $+0.52$, $+0.90$, and $+1.22$ V ($E_{1/2}$ against $E_{Ag/AgCl}$ in CH_2Cl_2 containing 0.1 M TBAP as the supporting electrolyte, see Supporting Information). To assign the redox states, **1** was subjected to spectroelectrochemical study using a platinum gauze OTTLE (optically transparent thin-layer electrode). However, the neutral form **1** is not stable because the peak intensities in the UV−vis spectra changed as a function of time prior to electrochemical control. The spectra exhibited isobestic points, suggesting the possibility of a redox reaction taking place in CH_2Cl_2. We thus prepared the one-electron oxidized form **3**, $[Ru_5(\mu_5\text{-tpda})_4Cl_2]\{[Ru_2(OAc)_4Cl]_2Cl\}$, by our previous protocol. Because the $[Ru_2(OAc)_4Cl]_2Cl$ anion complicates the voltammogram and UV−vis spectra, it was displaced by PF_6^-. The UV−vis spectra of the resulting $[Ru_5(\mu_5\text{-tpda})_4Cl_2](PF_6)$ are stable in CH_2Cl_2 and the voltammogram is identical to that of the neutral form **1**. The potential for the 1-e^- oxidation taking place is assigned to the potential range that yields spectroelectrochemical spectra identical to that of $[Ru_5(\mu_5\text{-tpda})_4Cl_2]^+$ acquired without potential control. Subsequently, other redox states can be determined. With this, the first oxidation potential (i.e., $E_{1/2}$(ox1) for $[Ru_5(\mu_5\text{-tpda})_4Cl_2]^{0/+}$) is determined to be at -0.11 V (versus $E_{Ag/AgCl}$). $E_{1/2,ox2}$ (at $+0.52$ V) and $E_{1/2,ox3}$ (at $+0.90$ V) for **1** are less positive than the respective reactions for $[Ru_3(dpa)_4Cl_2]$ at $+0.89$ and $+1.53$ V,[29] consistent with the trend that the longer the EMAC is, the easier for it is to undergo oxidation.[4,5]

The electrical conductance of a single molecule of $[Ru_5]^{10+}$ EMAC is determined by the method of STM (scanning tunneling microscopy) break-junction.[32–34] This requires anchoring of the molecular termini at the electrodes upon applying a bias voltage (E_{bias}) and monitoring the conducting current within the molecular junction. Therefore, for this study isothiocyanate was designed to be the axial ligand (i.e., complex **2**) and the anchoring group because of isothiocyanate's reasonable affinity toward gold surface.[32,33] The electrodes were the gold surface and a gold STM tip. Because of concerns of instability of **2** in solution, the measurements were carried out under an electrochemical environment. Panels a and b of Figure 4 were obtained when the working electrode was potentiostatted at $+200$ and -300 mV against $E_{Ag/AgCl}$, respectively, where the corresponding complexes were the one-electron oxidized and the neutral forms. Typical conductance traces are shown in the upper panels of Figure 4. The vertical axis is plotted in units of G_0 ($\sim(12.9\ k\Omega)^{-1}$), defined as the conductance quantum for a gold wire with the cross-section being only a single atom.[34–36] The conductance value decreases in a stepwise fashion while the STM tip is pulled away from the substrate. Each fall associated with the tip stretching indicates the loss of a molecule from the tip−substrate junction. The histogram of counts from more than one thousand traces shows local maxima at conductance values which are integer multiples of a fundamental one, suggesting that the number of molecules in the junctions was one, two, and so forth.[32–34] The conductance of a single molecule of the neutral form **2** is thus $2.4(0.5) \times 10^{-3}$ G_0, inferior to $[Cr_5(\mu_5\text{-tpda})_4(NCS)_2]$ $(3.9(0.8) \times 10^{-3}$ $G_0)$ but is more conductive than $[Co_5(\mu_5\text{-tpda})_4(NCS)_2]$ $(1.2(0.2) \times 10^{-3}$ $G_0)$ and $[Ni_5(\mu_5\text{-tpda})_4(NCS)_2]$ $(0.6(0.1) \times 10^{-3}$

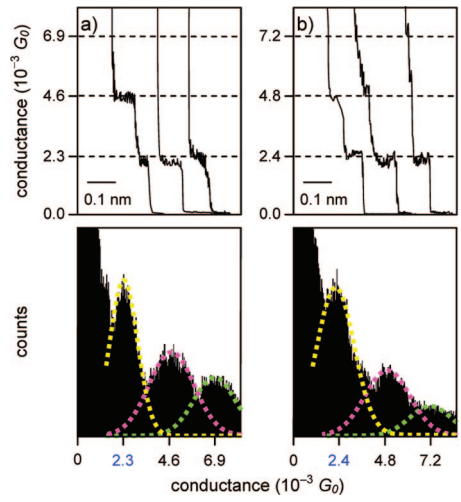

Figure 4. Electrical conductance of **2** measured by electrochemical STM break junction. The potentials were parked at (a) +200 mV and (b) −300 mV against $E_{Ag/AgCl}$ to produce predominantly one-electron oxidized and neutral forms of **2**, respectively. Upper panels: typical conductance-distance traces, with arbitrary *x* axis offsets, acquired upon stretching the molecular junction. Controlled experiments in blank dichloroethane yield exponential tunneling decay,[32–34] confirming that the staircase waveforms arose from **2**. Lower panels: the conductance histogram plotted from more than one thousand traces. The solution was 1 mM **2** dissolved in dichloroethane containing 0.1 M TBAP. The STM tip was insulated by polyethylene except the end of the tip to reduce the background noise. A Gaussian function was used to fit the histograms. The peak position and standard deviation of the Gaussian curve were used to find the single-molecule conductance and the uncertainty, respectively.

G_0). The conductance of **2** correlates quite well with the trend of bond orders which are 1.5, 0.5, and 0, respectively, for $[Cr_5]^{10+}$, $[Co_5]^{10+}$, and $[Ni_5]^{10+}$ EMACs. For $[Ru_5(\mu_5\text{-tpda})_4(NCS)_2]^+$, the conductance value of $2.3(0.5) \times 10^{-3}$ is essentially the same as the neutral form. On the basis of the bond order argument, the similar conductance indicates that the oxidized electron was removed from an orbital that has an insignificant contribution to the metal−metal interaction. From the calculated MO diagram (Figure 3), electronic states (Scheme S2), and the relative energy (Table S1), the most probable orbital for this oxidation is b_2 (i.e., δ^*, depicted in Figure 3). This is based on the following reasons: (1) b_2 (δ^*) is the highest occupied orbital, (2) δ and δ^* are considered nonbonding orbitals owing to the helical conformation of the $tpda^{2-}$ ligand, and (3) the removal of an electron from b_2 does not affect the molecular structure and thus the conductance much.

In summary, the first second-row metal EMAC was successfully synthesized with improved yields which made possible detailed characterization of its spectroscopy, magnetic properties, electrochemical redox states, and electrical conductance. Further investigation of EMACs with other second-row transition metals and with mixed metal centers are currently underway in our laboratory.

Acknowledgment. The authors thank MOE and NSC (ROC) for financial support, Mr. S.-C. Wang for SQUID measurements, Mr. L.-A. Lee for electrochemical measurements, and Drs. R. H. Ismayilov, W.-Z. Wang, and C.-L Hsieh for the fruitful discussions.

Supporting Information Available: Experimental procedures, spectroelectrochemical data, voltammograms, and the X-ray crystallographic files for compounds **1** and **2** (CIFs). This material is available free of charge via the Internet at http://pubs.acs.org.

References

(1) Aduldecha, S.; Hathaway, B. *J. Chem. Soc., Dalton Trans.* **1991**, 993–998.
(2) Pyrka, G. J.; El-Mekki, M.; Pinkerton, A. A. *J. Chem. Soc., Chem. Commun.* **1991**, 84–85.
(3) Wu, L.-P.; Field, P.; Morrissey, T.; Murphy, C.; Nagle, P.; Hathaway, B.; Simmons, C.; Thornton, P. *J. Chem. Soc., Dalton Trans.* **1990**, 3835–3840.
(4) Berry, J. F. Extended Metal Atom Chains. In *Multiple Bonds between Metal Atoms*; Cotton, F. A., Murillo, C. A., Walton, R. A., Eds.; Springer Science and Business Media: 2005; pp 669−706..
(5) Yeh, C.-Y.; Wang, C.-C.; Chen, C.-h.; Peng, S.-M. Molecular Metal Wires Built from a Linear Metal Atom Chain Supported by Oligopyridylamido Ligands. In *Redox Systems under Nano-Space Control*; Hirao, T., Ed.; Springer-Verlag: Berlin, Heidelberg, 2006; pp 85−116..
(6) Chien, C.-H.; Chang, J.-C.; Yeh, C.-Y.; Lee, G.-H.; Fang, J.-M.; Peng, S.-M. *Dalton Trans.* **2006**, 2106–2113.
(7) Chien, C.-H.; Chang, J.-C.; Yeh, C.-Y.; Lee, G.-H.; Fang, J.-M.; Song, Y.; Peng, S.-M. *Dalton Trans.* **2006**, 3249–3256.
(8) Liu, I. P.-C.; Benard, M.; Hasanov, H.; Chen, I-W. P.; Tseng, W.-H.; Fu, M.-D.; Rohmer, M.-M.; Chen, C.-h.; Lee, G.-H.; Peng, S.-M. *Chem.—Eur. J.* **2007**, *13*, 8667–8677.
(9) Lopez, X.; Huang, M.-Y.; Huang, G.-C.; Peng, S.-M.; Li, F.-Y.; Benard, M.; Rohmer, M.-M. *Inorg. Chem.* **2006**, *45*, 9075–9084.
(10) Tsao, T.-B.; Lo, S.-S.; Yeh, C.-Y.; Lee, G.-H.; Peng, S.-M. *Polyhedron* **2007**, *26*, 3833–3841.
(11) Chen, Y.-H.; Lee, C.-C.; Wang, C.-C.; Lee, G.-H.; Lai, S.-Y.; Li, F.-Y.; Mou, C.-Y.; Peng, S.-M. *Chem. Commun.* **1999**, 1667–1668.
(12) Cotton, F. A.; Daniels, L. M.; Murillo, C. A.; Pascual, I. J. *Am. Chem. Soc.* **1997**, *119*, 10223–10224.
(13) Cotton, F. A.; Daniels, L. M.; Murillo, C. A.; Wang, X.; Murillo, C. A. *Chem. Commun.* **1999**, 2461–2462.
(14) Ismayilov, R. H.; Wang, W.-Z.; Wang, R.-R.; Yeh, C.-Y.; Lee, G.-H.; Peng, S.-M. *Chem. Commun.* **2007**, 1121–1123.
(15) Clerac, R.; Cotton, F. A.; Dunbar, K. R.; Lu, T.; Murillo, C. A.; Wang, X. *J. Am. Chem. Soc.* **2000**, *122*, 2272–2278.
(16) Shieh, S.-J.; Chou, C.-C.; Lee, G.-H.; Wang, C.-C.; Peng, S.-M. *Angew. Chem., Int. Ed. Engl.* **1997**, *36*, 56–59.
(17) Lai, S.-Y.; Lin, T.-W.; Chen, Y.-H.; Wang, C.-C.; Lee, G.-H.; Yang, M.-h.; Leung, M.-k.; Peng, S.-M. *J. Am. Chem. Soc.* **1999**, *121*, 250–251.
(18) Lai, S.-Y.; Wang, C.-C.; Chen, Y.-H.; Lee, C.-C.; Liu, Y.-H.; Peng, S.-M. *J. Chin. Chem. Soc.* **1999**, *46*, 477–485.
(19) Peng, S.-M.; Wang, C.-C.; Jang, Y.-L.; Chen, Y.-H.; Li, F.-Y.; Mou, C.-Y.; Leung, M.-k. *J. Magn. Magn. Mater.* **2000**, *209*, 80–83.
(20) *Comprehensive Coordination Chemistry II: From Biology to Nanotechnology*, 2nd ed.; McCleverty, J. A., Meyer, T. J., Eds.; Elsevier Science: Oxford, 2003.
(21) Ren, T. *Organometallics* **2005**, *24*, 4854–4870.
(22) Newkome, G. R.; Cho, T. J.; Moorefield, C. N.; Mohapatra, P. P.; Godinez, L. A. *Chem.—Eur. J.* **2004**, *10*, 1493–1500.
(23) Otsuki, J.; Akasaka, T.; Araki, K. *Coord. Chem. Rev.* **2008**, *252*, 32–56.
(24) Stephenson, T. A.; Wilkinson, G. *J. Inorg. Nuclear Chem.* **1966**, *28*, 2285–2291.
(25) Bennett, M. J.; Caulton, K. G.; Cotton, F. A. *Inorg. Chem.* **1969**, *8*, 1–6.
(26) Xu, G.; Ren, T. *Inorg. Chem.* **2001**, *40*, 2925–2927.
(27) Angaridis, P. Ruthenium Compounds. In *Multiple Bonds between Metal Atoms*; Cotton, F. A., Murillo, C. A., Walton, R. A., Eds.; Springer Science and Business Media: 2005; pp 377−430..
(28) Sheu, J.-T.; Lin, C.-C.; Chao, I.; Wang, C.-C.; Peng, S.-M. *Chem. Commun.* **1996**, 315–316.
(29) Kuo, C.-K.; Liu, I. P.-C.; Yeh, C.-Y.; Chou, C.-H.; Tsao, T.-B.; Lee, G.-H.; Peng, S.-M. *Chem.—Eur. J.* **2007**, *13*, 1442–1451.
(30) An oxidized pentaruthenium, $[Ru_5(\mu_5\text{-tpda})_4Cl_2]\{[Ru_2(OAc)_4Cl]_2Cl\}$, was obtained at a low yield (< 1%) when employing the protocol that the metalation of H_2tpda deprotonation was carried out after 2 hr reflux of $Ru_2(OAc)_4Cl$], H_2tpda, and excess LiCl. The anion, $\{[Ru_2(OAc)_4Cl]_2Cl\}$, was a dimer of the starting ruthenium salt bridged by a chloride. The characterization of this compound was hampered by the low yield.
(31) Kahn, O. *Molecular Magnetism*; VCH: New York, 1993.
(32) Fu, M.-D.; Chen, I-W. P.; Lu, H.-C.; Kuo, C.-T.; Tseng, W.-H.; Chen, C.-h. *J. Phys. Chem. C* **2007**, *111*, 11450–11455.
(33) Chen, I-W. P.; Fu, M.-D.; Tseng, W.-H.; Yu, J.-Y.; Wu, S.-H.; Ku, C.-J.; Chen, C.-h.; Peng, S.-M. *Angew. Chem., Int. Ed.* **2006**, *45*, 5814–5818.
(34) Xu, B.; Tao, N. J. *Science* **2003**, *301*, 1221–1223.
(35) Yanson, A. I.; Bollinger, G. R.; van den Brom, H. E.; Agrait, N.; van Ruitenbeek, J. M. *Nature* **1998**, *395*, 783–785.
(36) Ohnishi, H.; Kondo, Y.; Takayanagi, K. *Nature* **1998**, *395*, 780–783.

JA8016818